ov 2025 I Iron & Steel Technology I AIST.org

The Role of Nb and Coiling Temperature on Heavy-Gauge X80 Line Pipe Steel Strength and Toughness





The interaction of Nb content and coiling temperature is important to properties such as strength and low-temperature toughness of heavy-gauge (≥22 mm) X80 line pipe steels. In this study, two levels of Nb are examined as well as two different coiling temperatures for the alloy with a lower level of Nb through the use of pilot-scale vacuum induction melting, casting, rolling and coiling thermal simulations. Tensile testing is completed and also drop weight tear testing, which was performed at two temperatures and orientations. Microstructural characterization provides insight into the differences observed from tensile and fracture testing.

Authors

Michael J. Gaudet (left), Manager of Metallurgy, R&D, Interpro Pipe and Steel, Regina, Sask., Canada michael.gaudet@interprosteel.com

Muhammad Rahman (right), formerly of Interpro Pipe and Steel, Regina, Sask., Canada

Peter Poruks, Senior Research Engineer, Interpro Pipe and Steel, Regina, Sask., Canada peter.poruks@interprosteel.com

Fateh Fazeli, Research Scientist, CanmetMATERIALS, Natural Resources Canada, Hamilton, Ont., Canada fateh.fazeli@nrcan-rncan.gc.ca

Muhammad Rashid, Senior Program Manager, Interpro Pipe and Steel, Regina, Sask., Canada muhammad.rashid@interprosteel.com

Muhammad Arafin, Vice President R&D North America, Orion Steel Companies, Chicago, III., USA muhammad.arafin@orionsteel.com

Introduction

Pipeline designs intended for lowtemperature environments are more economically feasible when designed and constructed with heavier gauges and higher-strength steel grades (e.g., API X80).^{1,2} Such grades and pipe wall thicknesses are achieved through alloying and thermomechanicalcontrolled processing (TMCP). Particularly, a microalloying approach, often utilizing Nb, with optimized TMCP is important not only to achieve the needed strength and gauges but it also provides a method to obtain good lowtemperature fracture toughness such as determined through the drop weight tear test (DWTT).1 However, moving to a greater wall thickness of the steel line pipe creates greater challenges on the design of the alloy and the TMCP to mitigate issues such increased rolling forces, larger gradients through thickness temperature and strain, and so on.^{3,4} Additionally, spiral-formed line pipe utilizes coils. The TMCP after accelerated cooling requires the strip to then be coiled at an elevated temperature which may have certain consequences on the microstructure and properties.^{5–7} Thus, to achieve good strength and good lowtemperature toughness at greater wall thicknesses in steel for spiral line pipes,

both alloy designs and TMCP parameters need optimization.

As a microalloying element, Nb has a strong influence on the microstructure evolution during each stage of TMCP and thus has direct and indirect impact on the final microstructure and properties.¹ The Nb can be found in solid solution as a substitutional element or in precipitates as a carbide (NbC), nitride (NbN), or carbonitride (NbCN). Both forms of Nb (in solution or in precipitates) have effects on the evolution of the austenite (y) during hot rolling, influencing aspects such as recrystallization, strain accumulation and austenite decomposition (transformation) during accelerated cooling.^{8–10} Also, fine precipitates of NbC can significantly enhance the strength of the final line pipe steel while both fine and coarse or undissolved NbC are detrimental to toughness. As Nb content significantly influences the precipitation of NbC, it is of interest to understand fully.

The coiling temperature also has an influence on the final microstructure and properties of the steel. In cases where γ decomposition has not fully completed on the runout table (e.g., not low enough coiling temperature or time), enrichment and transformation occur differently than under continuous cooling.⁵ This can lead to

Based on a design for a spiral-formed X80 heavy-gauge line pipe (22.2 mm, 0.875 inch), this study uses pilot-scale casting and rolling to consider the effects of two Nb levels and different coiling temperatures. Tensile testing and DWTT are performed to determine the mechanical and fracture properties of the steel. Microstructure and texture characterization provide insight into the differences between the Nb level and coiling temperature effects.

Table 1

Measured Alloy Content of CMAT Pilot-Scale Cast Steels (wt. %)

Steel	С	Nb	Mn+Ni+Cr+Si	Ti+Mo+V
Nb9-M	0.053	0.092	2.29	0.323
Nb6-H	0.050	0.060	2.32	0.323
Nb6-L	0.052	0.059	2.31	0.323

Methodology

Material and TMCP

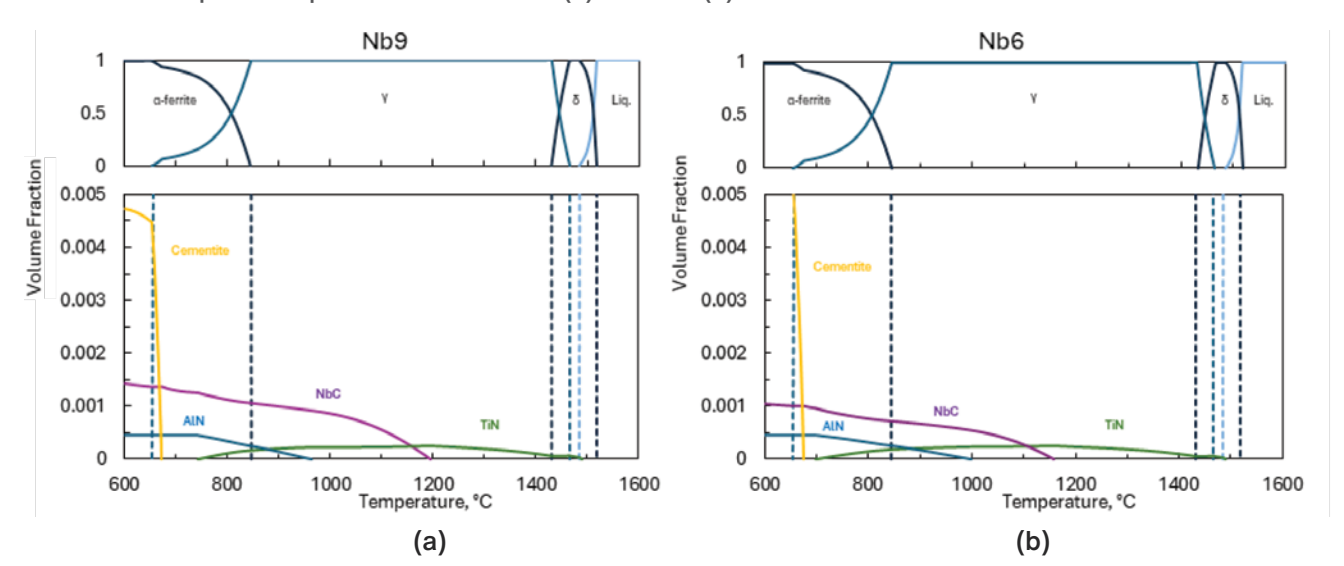
steel for this work was generated CanmetMATERIALS (CMAT) in a vacuum induction melting (VIM) furnace and cast into a static mold to produce ingots with the target chemistry. The reheating of the trimmed VIM ingots was carried out under Ar to reduce scale formation ahead of rolling. The TMCP was carried using CMAT's single-stand reversing mill with on-line accelerated cooling (OLAC). Coiling was simulated using furnaces set at target temperature and then allowed to furnace cool. For the pilot-scale rolling, the industrial TMCP design from a slab with a thickness of 254 mm (10 inches) to a final strip thickness of 22.2 mm (0.875 inch) was scaled down at CMAT by rolling from an ingot thickness of 203.2 mm (8.0 inches) to 17.8 mm (0.70 inch) with the width of the strip being 203.2 mm (8.0 inches).

A microalloyed approach was used, varying only by the Nb level. Two levels of Nb were selected with the high and low levels being 0.09 wt. % Nb and 0.06 wt. % Nb, or Nb9 and Nb6 in short. Other alloying elements were also used, such as Mn, Si, Ti, etc. These alloys were subjected to high (H), medium (M) or low (L) coiling temperatures, given steels the designations of Nb9-M, Nb6-H and Nb6-L. The compositions are given in Table 1 while Fig. 1 shows the full results of the Thermo-Calc equilibrium phase prediction for the two systems. ¹³

The TMCP practices were kept similar for this study except coiling temperature. The reheat temperature used was less than 1,200°C was selected for this study. The Thermo-Calc results suggest the reheat temperature was above the NbC solubility temperature for the

Figure 1

Thermo-Calc equilibrium phases for steels Nb9 (a) and Nb6 (b).



low-Nb cases (Nb6). However, for the high Nb (Nb9), the Thermo-Calc results suggest there may be some incomplete dissolution of the NbC.

A delay between the end of roughing and start of finishing was used to avoid partial recrystallization during rolling as determined by the nonrecrystallization (T_{nr}) and recrystallization stop (T_r) temperatures. The T_{nr} and T_r were determined according to:¹⁴

$$T_{mr}$$
 (°C) = 174 · log $\left(Nb \cdot \left[C + \frac{12}{14}N\right]\right) + 1444$ (Eq. 1)

$$T_{nr} (^{\circ}C) = T_{nr} - 75$$
 (Eq. 2)

where Nb, C and N are given in wt. %. For the high-Nb and low-Nb steels, this gave a T_{nr} of ≈1,045°C and ≈1,010°C, respectively, and a T_r of ≈970°C and ≈935°C, respectively. Consequently, the last roughing surface temperature was above 1,045°C and the first finishing surface temperature was below 935°C.

The equilibrium prediction for ferrite formation (Ae₃) from Thermo-Calc gives values of ≈850°C for both the high- and low-Nb approaches. With some consideration of kinetics, the Ouchi predicted start temperature of α -ferrite formation (Ar₃) as determined in Eq. 3 is useful.15

Figure 2

Schematic of the thermomechanical-controlled processing (TMCP) designs.

$$Ar_{3}(^{\circ}C) = 910 - 310 \cdot C - 80 \cdot Mn - 20 \cdot Cu$$
$$-15 \cdot Cr - 55 \cdot Ni - 80 \cdot Mo + 0.35 \cdot (t - 8)$$
(Eq. 3)

where the elements are provided in wt. % and t is thickness of the strip in mm. As Nb is not considered, the Ar₃ predicted is similar among the steels and is ≈725°C. The last finishing pass occurred at a surface temperature above 725°C but below 850°C.

Previous work using dilatometry and hardness measurements to study simulated coiling temperatures and hold times showed that the hardness increased over time (between 10 minutes and 60 minutes) for a hold temperature even as low as 450°C.⁵ Thus, a moderate coiling temperature (≈500°C) was used for the high-Nb steel, while the low-Nb steels applied a high coiling temperature (≈550°C) and a low coiling temperature (≈450°C). A schematic of the TMCP design is shown in Fig. 2.

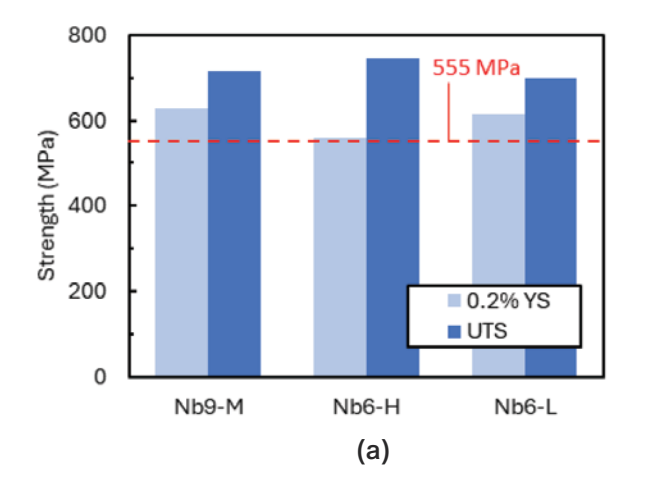
Mechanical and Fracture Testing

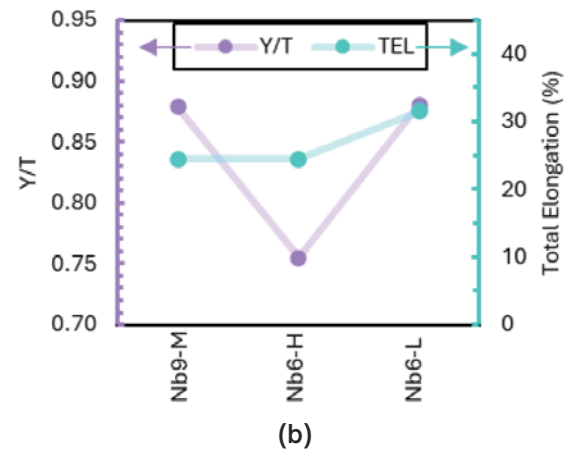
Tensile testing at ambient temperature were carried out using transverse to rolling direction (TRD) specimens taken from the plates to investigate the strength and ductility. These were machined to a subsize sample with a gauge length of 50 mm and width of 12.5 mm, and a full plate thickness of 17.8 mm. A dual-speed procedure according to ASTM A370 was used for the test where the initial crosshead speed is 3 mm/minute (0.001/second) and the second-stage speed is 25 mm/minute (0.008) second). Two samples per condition were tested with the 0.2% offset yield strength used in the analysis.

DWTT according to API RP 5L3 was used to assess the steels in this study. 16 As in previous works, DWTT specimens were machined at full thickness with the

> length along the longitudinal rolling direction (LRD) and notched in the TRD of the skelps. In addition to these LRD samples, CMAT's new furnace allowed for a full strip to be used resulting in capacity to generate more samples. As spiral line pipe uses a DWTT orientation that is transverse to pipe axis (TPA) and is offset of the LRD, this study also sampled DWTTs that were oriented at 30° to the LRD (herein called +30°). Both the LRD and +30° samples used a pressed notch and were conducted using a set of two tests for each condition at testing temperatures of -20°C and –45°C. Percentage of ductile shear area (%SA) was determined through photographing the surface and measuring the surface using the Fiji distribution of ImageJ.¹⁷

Tensile properties of strength (a); Y/T ratio and total elongation percent (TEL) (b).





Microstructure Characterization

Metallography samples were sectioned on the LRD-normal direction (LRD-ND) cross-section. The microstructures were examined using 2% Nital etching to observe the general features. LePera etching was used to reveal by optical microscopy. The average volume fraction and size of these phases were analyzed at the quarter thickness and centerline of the skelps with three measurements at each location using a brightness threshold analysis.

Scanning electron microscopy (SEM) with secondary electron (SE) and backscattered electron (BSE) imaging was used in general surveys. Also, the electron backscattered diffraction (EBSD) technique allowed for microstructure and microtexture quantification as performed by the characterization group at CMAT.

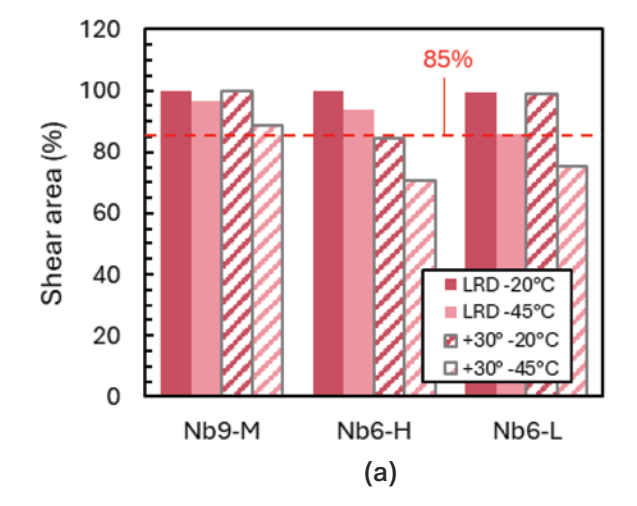
Results and Discussion

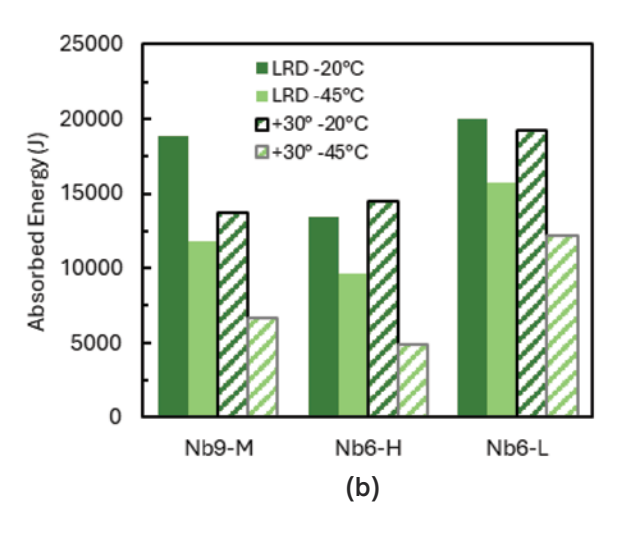
Mechanical and Fracture Properties

The results of the tensile testing are summarized in Fig. 3. The standout was Nb6-H, which had the lowest yield strength (YS), highest ultimate tensile strength (UTS) and therefore lowest Y/T ratio by far of the three cases. The highest YS (628 MPa) is observed in the Nb9-M case. The Nb6-L steel had a yield strength (YS) and UTS just slightly lower than Nb9-M. However, the measured total elongation of Nb6-L was better than that of Nb9-M and Nb6-H. There is a stark difference between Nb6-H and Nb6-L in tensile performance, indicating that there is a strong impact of the coiling temperature over this range. Keeping this in consideration when assessing the moderate coiling temperature in the Nb9-M steel, it seems that

Figure 4

Drop weight tear test (DWTT) results: shear area percentage (%SA) (a) and absorbed energy (b).





there could be potential for higher strengths at this Nb level should a lower coiling temperature be made. While the stress-strain curves are not shown here, the low Y/T of Nb6-H in this case was associated with a rounded stress-strain response whereas both Nb9-M and Nb6-L showed yield point elongation behavior. Also, the low YS of Nb6-H (558 MPa) is above the requirements of X80 steel (555 MPa). However, in real production, this TRD skelp would need to be formed into spiral pipe, in which case the forming and angle for the TPA test would likely drop the effective strength. Consequently, Nb6-H is at risk of not making strength in production.

The DWTT shear area percentage (%SA) and absorbed energy of both the LRD and the +30° samples are shown in Fig. 4. According to API 5L3, an average of 85% shear area is needed to pass. The best %SA performance was in Nb9-M including closely passing the +30° sample at a temperature of -45°C. The Nb6-H case also performed well in the LRD samples according to %SA. However, despite its lower yield strength, Nb6-H fell behind in performance of the other two conditions in the +30° samples as it failed both the -20°C and -45°C tests. The only failure in the LRD samples came from Nb6-L at -45°C. In terms of absorbed energy, the Nb6-L strongly outperformed the other cases across all samples and test temperatures. The effect of +30° is seen in the %SA, where

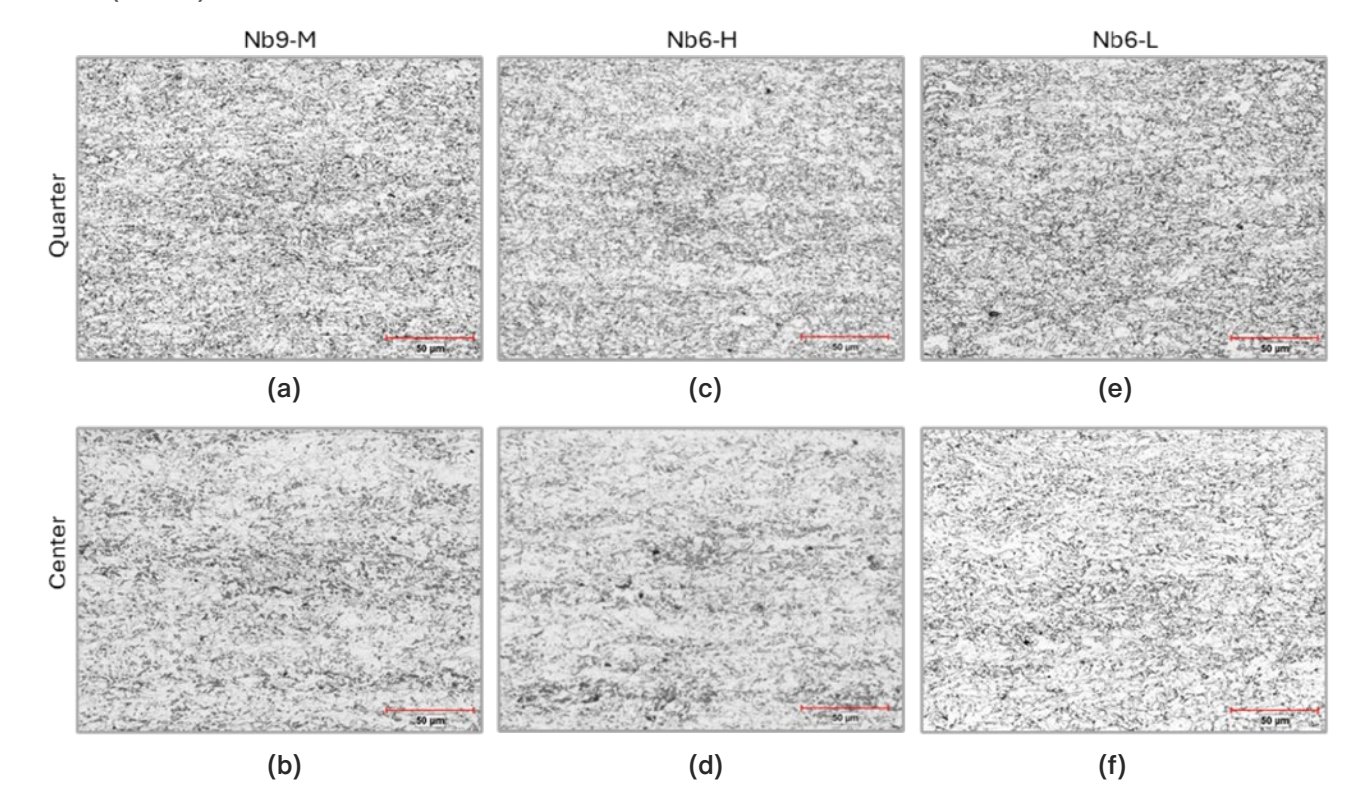
these samples performed worse than the LRD samples, as expected. The same is true for the DWTT energy results, except in the case for Nb6-L, which shows a slightly higher absorbed energy for the +30° test at -20°C. This indicates the +30° samples should provide a more realistic assessment of production TPA DWTT performance.

Microstructure Characterization

Characterization of the microstructures was performed at the quarter thickness (QT) from the top of the plate and at the centerline (CL) of the plate. Fig. 5 shows the nital-etched microstructures that demonstrates a fine microstructure consisting primarily of acicular ferrite and quasi-polygonal ferrite grains in all cases. In all steels, the QT microstructures are finer than the CL with the CL of Nb6-H and Nb9-M showing a considerable number of darker phases that are often found to be martensite/ retained austenite (M/A), pearlite or degenerate pearlite structures. The EBSD analysis is used to determine the grain size distribution and average grain size utilizing a 15° misorientation criteria as given in Fig. 6. This confirms the observation of the finer grain sizes of the QT location as compared to the CL for Nb9-M and Nb6-H. These steels show a finer QT grain size than Nb6-L. At the CL position, Nb6-H showed a slightly larger grain size. Both Nb9-M and Nb6-H show a number of

Figure 5

Nital-etched microstructures at quarter thickness (QT) and centerline (CL) of Nb9-M (a and b), Nb6-H (c and d) and Nb6-L (e and f).



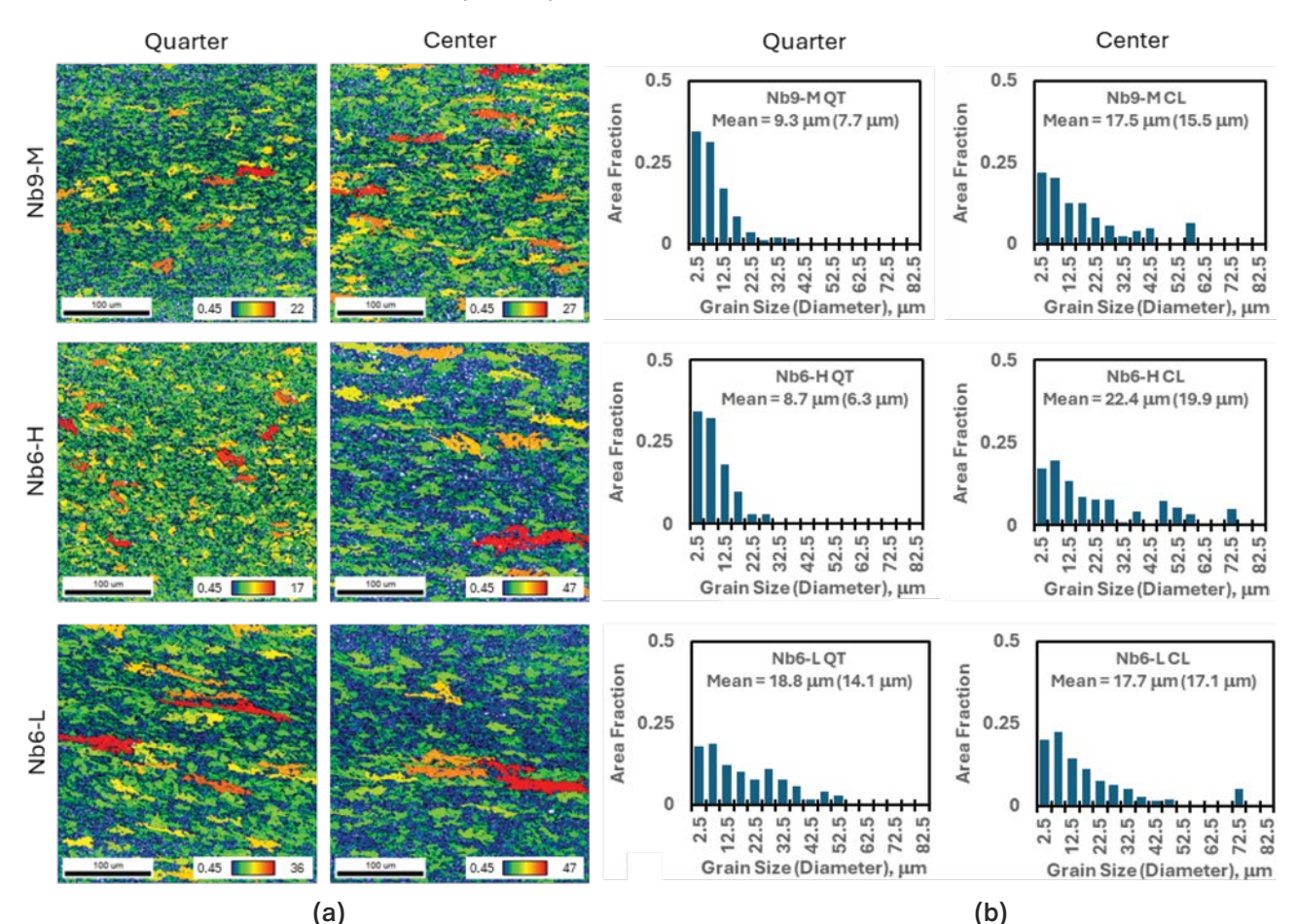
Grain shape aspect ratio (GSAR) is used to determine the extent of elongated structures in the structure that may be detrimental to toughness. The GSAR maps at the QT and CL are presented in Fig. 7 along with the GSAR distributions for each steel, where values of 1 would be an equiaxed or round grain and lower values would therefore indicate elongated structures. In Nb6-L, the more elongated grain structure at the QT is evident. However, the GSAR heterogeneity between QT and CL as seen by the distributions appears to be less for Nb6-L compared to the other cases. A noticeable heterogeneity in GSAR is observed in Nb6-H where its QT shows a less elongated structure, while the CL shows the distribution moving to lower GSAR values. A shift in the GSAR is also observed

in Nb9-M. As with the grain size, the situation for Nb6-L here stands out and may be related to the larger elongated grains found in the scan, likely owing to the combination of processing and cooling this steel received.

Dislocation density is an important factor in the strength and toughness of line pipe steels. From the EBSD scans, the geometrically necessary dislocation (GND) density was determined based on the kernel average misorientation (KAM) using the first nearest neighbor analysis. The KAM maps at the QT and CL for all steels and the resulting GND density distributions are given in Fig. 8. In the Nb9-M steel, a slightly greater GND density is observed at the QT as compared to the CL of the material while Nb6-H maintained a consistent GND density at both locations. The GND density for the QT of Nb6-L is the lowest observed, though it shifted significantly from the QT to the CL, which suggests there is a more significant heterogeneity of dislocations in this steel.

Figure 6

EBSD using 15° misorientation thresholding for grain size maps (a) and grain size distributions (b) with listed mean sizes and standard deviations for Nb9-M, Nb6-H, and Nb6-L.



2025 I Iron & Steel Technology I AIST.org

Secondary Phase Characterization

Technical Article

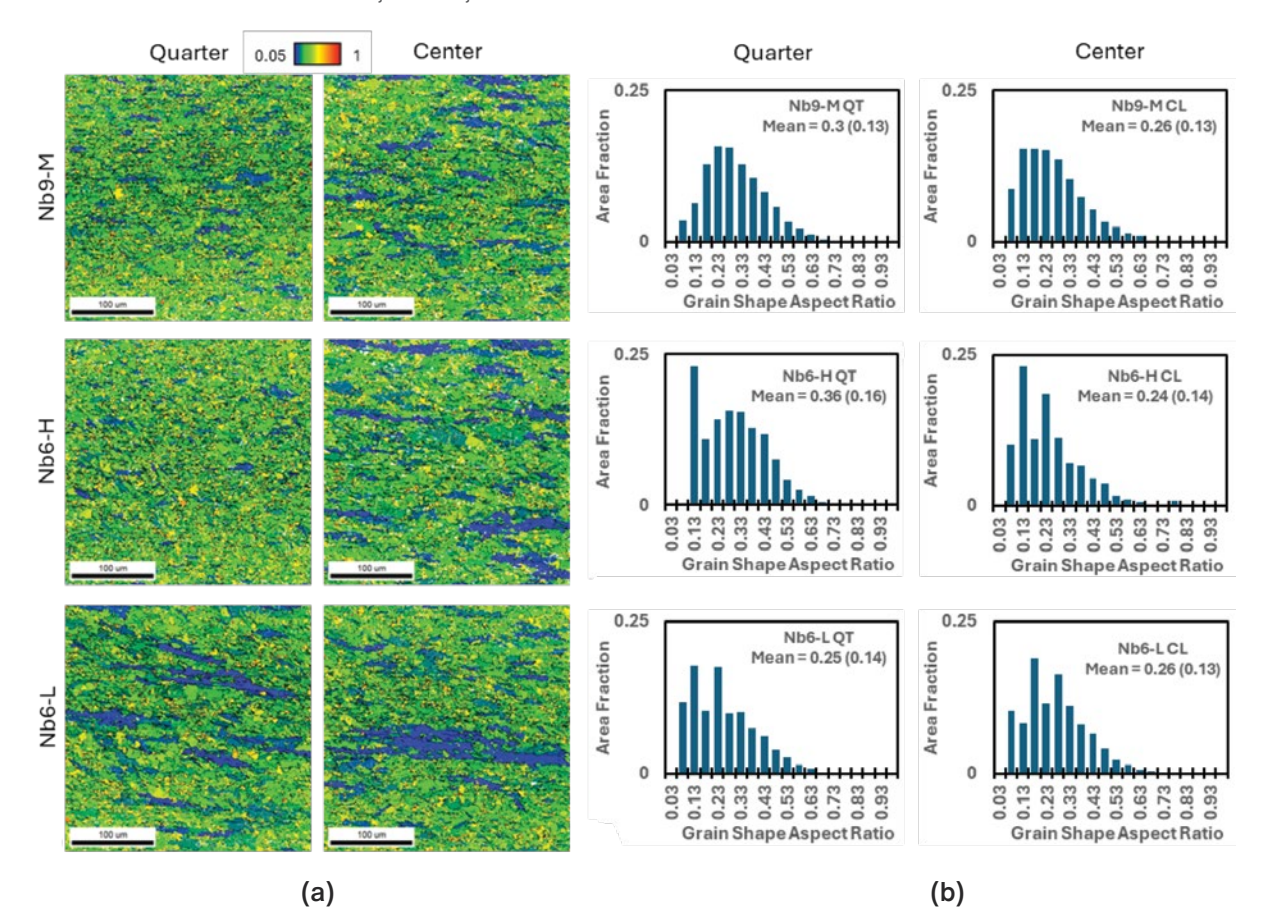
Typical of these steels, some amount of M/A, pearlite and degenerate pearlite can be found in the microstructure.⁴ Here, LePera etching was used to expose the M/A and other nonetched secondary phases to be observed as white areas when observed with light optical microscopy. Representative images at the QT and CL of the LePera-etched samples are shown for all cases in Fig. 9. Quantification of the secondary phases is given in Fig. 10. Interestingly, Nb6-L shows very little secondary phases present compared to the other cases. This sample was subjected to multiple repolishing and re-etching attempts that resulted in comparable results each time. This shows the lower coiling temperature was effective in controlling the evolution of these secondary phases in the Nb6-L, suggesting that these phases may be related to the final proportion of γ decomposition. It is likely that the DWTT performance of Nb6-L was improved through the lower amount of these secondary phases. While both Nb9-M and Nb6-H show both more numerous and larger secondary phases than Nb6-L, their distributions through thickness are different. While Nb9-M has a

greater amount of secondary phases at the CL, Nb6-H has a greater proportion at the QT. Assuming the threequarter thickness is similar to the QT, this suggests there is a significantly greater amount of these secondary phases across the thickness of the Nb6-H steel, influencing its properties and likely worsening its DWTT performance.

As noted earlier, the reheat temperature used in this study was below the calculated solubility temperature for Nb9-M. As part of regular investigations into all cases, a survey was carried out on the nital-etched microstructure of this steel to determine if there were any undissolved coarse NbC. Fig. 11 demonstrates a case of a large Nb-containing particle that was found. In this case, this particle was examined using energy-dispersive spectroscopy (EDS) and was found to be associated with a large amount of Ti and thus likely was related to a thermally stable TiN that formed during casting. Similar particles are typically found even in cases where reheat temperatures were above the NbC dissolution. However, no extensive amounts of large NbC were found throughout the section observed, which suggests that the NbC was mostly dissolved during reheating. That said, there

Figure 7

EBSD grain shape aspect ratio (GSAR) maps (a) and GSAR distributions (b) with listed mean ratios and standard deviations for Nb9-M, Nb6-H, and Nb6-L.



EBSD kernel average misorientation (KAM) maps (a) and GND density distributions (b) with listed mean densities and standard deviations for Nb9-M, Nb6-H, and Nb6-L.

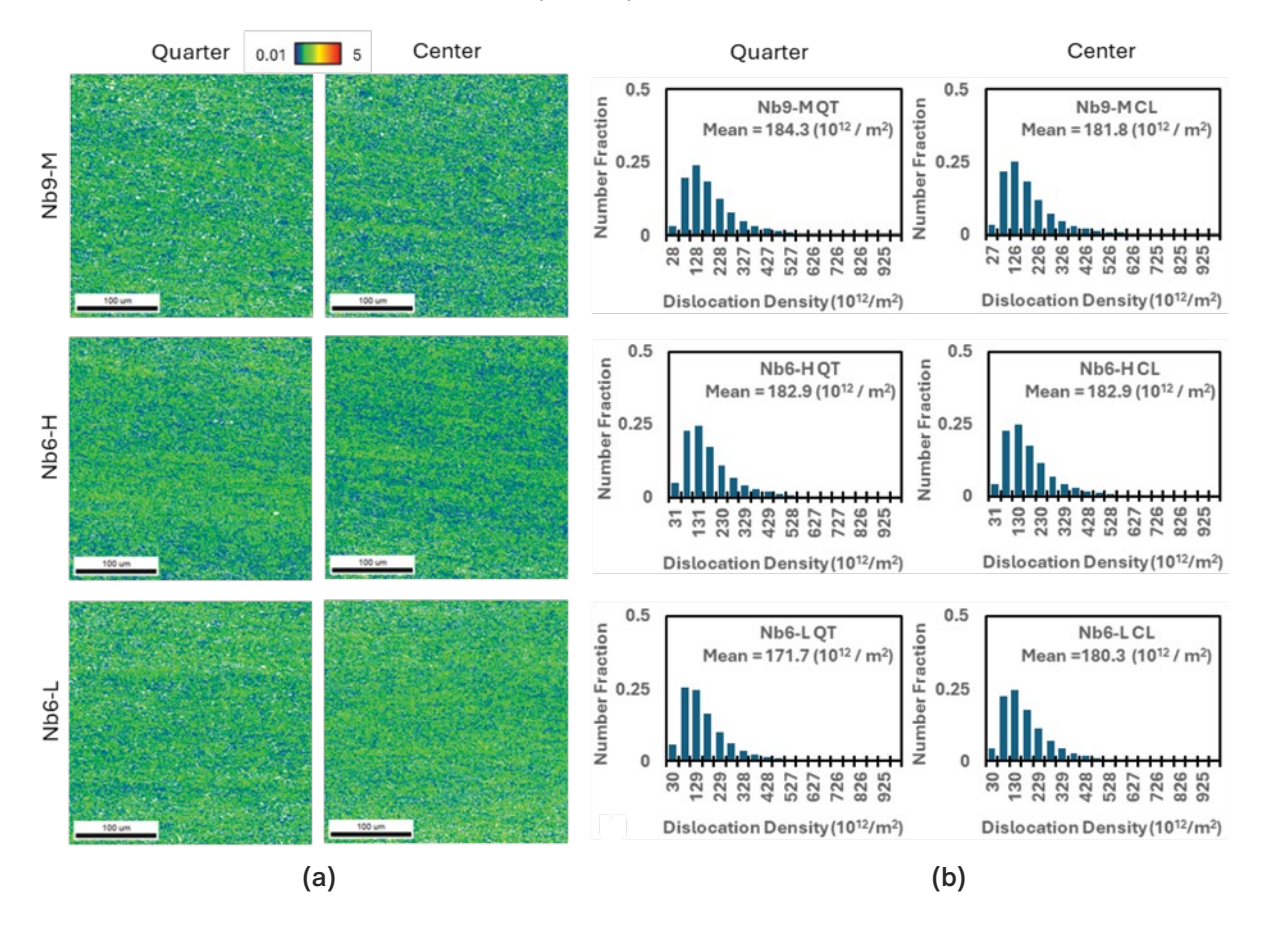


Figure 9

LePera etched microstructures at QT and CL for Nb9-M, Nb6-H, and Nb6-L.

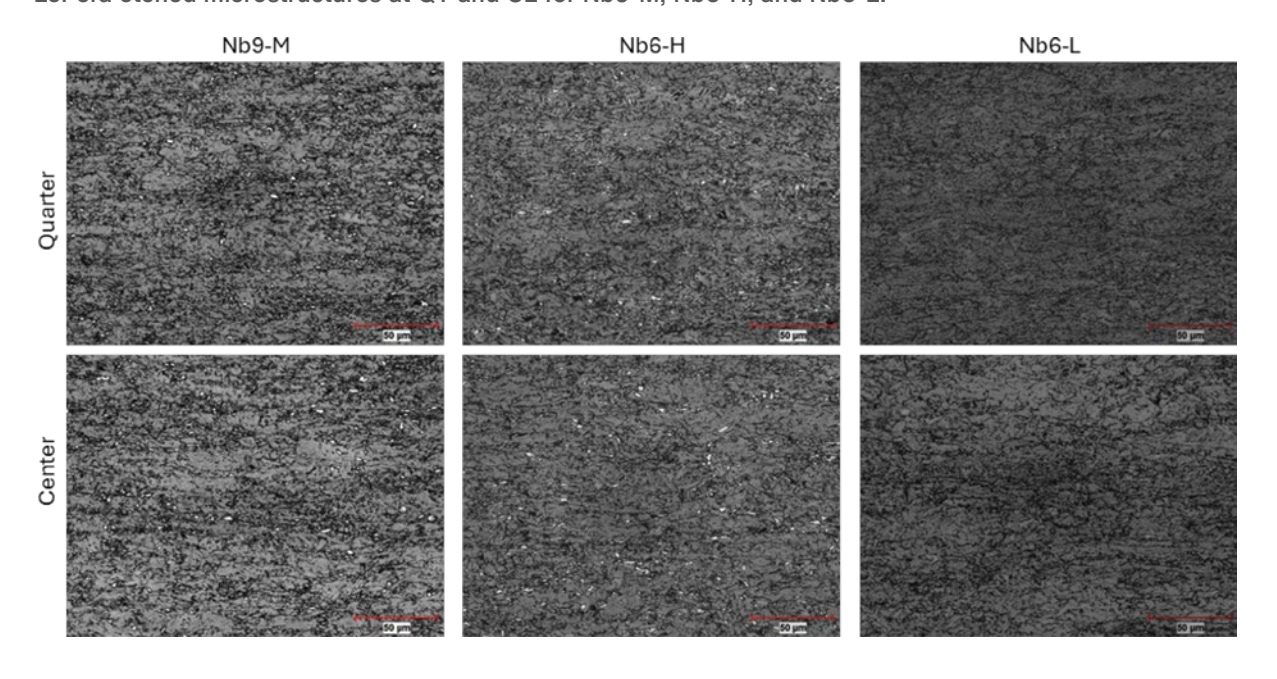


Figure 10

Secondary phases area distributions with summarized mean areas and average area percentage with standard deviations for Nb9-M, Nb6-H, and Nb6-L.

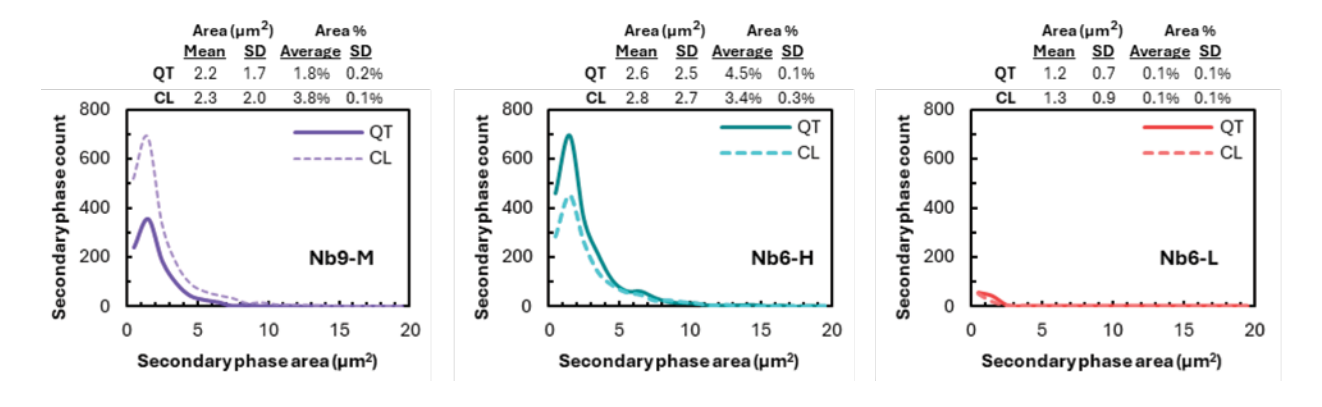
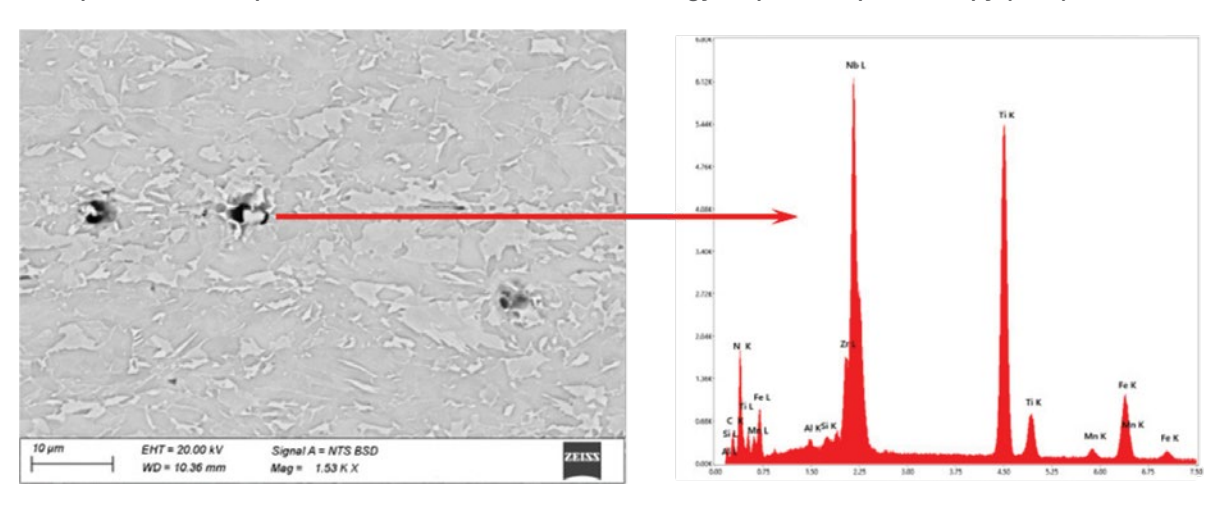


Figure 11

Example of a coarse particle in Nb9-M and associated energy-dispersive spectroscopy (EDS) result.



remains the possibility that coarse NbC remained in the microstructure but not found in the section observed in this work.

Microtexture

The EBSD scans were used to assess the microtexture of the steels as texture is known to have an effect on toughness in line pipe steels. ^{18,19} Expected texture components of line pipe steel were observed including the α -fiber (containing rotated cube, transformed copper textures), γ -fiber and ϵ -fiber (associated with {332}<113> component). Of particular interest is the {001}<110> component (rotated cube) since it is expected to be detrimental to fracture toughness and may have delamination or splits related to the weakest {001} planes in the BCC ferrite structure. ¹⁹ On the other hand, good toughness has correlation to the {332}<113> texture component. ¹⁹ Fig. 12

shows the orientation distribution function (ODF) maps for all steels at the QT and CL with ϕ_2 of 0° and 45°. All steels showed some presence of the rotated cube component. The texture of Nb6-H was differing significantly at the QT compared to the other cases, here showing a strong {001}<210> component. In the case of Nb6-L, the overall intensities were similar between QT and CL, though a more significant transformed brass component is seen at the QT. The texture of Nb9-M was more consistent and showing some presence of {332}<113> at both the QT and CL. The {332}<113> was also seen in the CL of Nb6-H, but the overall texture was weak.

Conclusions

Steels with an alloy designed for heavy-gauge line pipe (22.2 mm equivalent gauge) with X80 strength and good

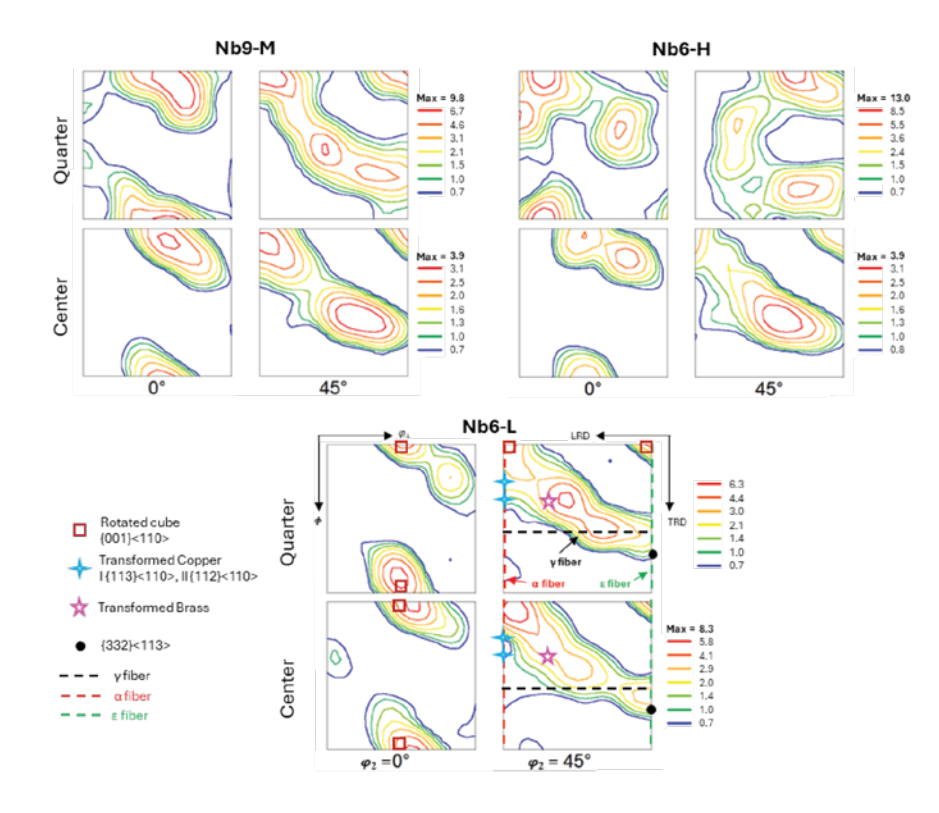
Nov 2025 I Iron & Steel Technology I AIST.org

low-temperature toughness were pilot-scale cast and TMCP rolled. Of these steels, one had a Nb level of either 0.09 wt. % and a medium coiling temperature (Nb9-M), while the 0.06 wt. % Nb steels were coiled at high and low temperatures (Nb6-H, Nb6-L). Tensile tests and DWTT were carried out with the DWTT being performed with two orientations, LRD and +30° to LRD, and at two temperatures, -20°C and -45°C. Microstructure evaluations were performed using nital and LePera etching along with optical microscopy and quantification of key features and microtexture by EBSD. Significant differences in properties and microstructures were observed among the three steels. To conclude:

- 1. The YS of Nb9-M and Nb6-L were 628 MPa and 614 MPa, respectively. These steels were comfortably above the X80 YS requirement of 555 MPa. With a YS of 558 MPa, Nb6-H mar
 - ginally passed the level though expected strength drops from forming spiral line pipe would likely mean this condition would fail in practice.
- 2. The UTS of Nb6-H was 747 MPa 31 MPa higher than that of Nb9-M. Consequently, Nb6-H had the lowest Y/T of the three steels while also being the only steel not to exhibit yield point elongation.
- 3. Drop weight tear test had the best performance from Nb9-M on the basis of %SA. While Nb6-L also performed decently at -20°C, it had a failure with the +30° samples at -45°C. It also had higher absorbed energy values, which suggests that there could be capacity for improved toughness with the Nb6-L strategy. Also, several microstructure factors appear to favor the Nb6-L approach. In any case, both Nb9-M and Nb6-L have merits for further optimization. In contrast, the Nb6-H steel performed the worst of the three despite having the lowest YS.
- 4. All steels showed a fine-grained structure consisting mainly of acicular ferrite and quasipolygonal ferrite. The finest grain sizes were observed in Nb9-M which supports its high

Figure 12

Orientation distribution function (ODF) maps at QT and CL for Nb9-M, Nb6-H, and Nb6-L.



- strength and good DWTT performance. Larger grain sizes were observed in Nb6-L though there was less of a difference between quarter thickness and centerline and thus exhibited less grain size heterogeneity.
- 5. Secondary phases (e.g., M/A) as observed with LePera etching were extremely limited in the Nb6-L. This was likely due to the low coiling temperature and subsequently was favorable to its good DWTT performance.
- 6. The microtexture observed in the steels varied significantly though remained relatively weak overall with all steels showing some presence of the rotated cube texture. Supporting its good toughness, Nb9-M showed some presence of the beneficial {332}<113> texture component which was stronger at the QT.

Acknowledgment

There are a great number of supporting partners for this work: The EVRAZ NA R&D (now Interpro Pipe and Steel) technologists, staff, and students who were critical to the sample preparation, testing, and characterization work. Also, the Regina Tubular QA Lab supported the

DWTT testing performed here. Technical support and contribution of casting, rolling and characterization team of CanmetMATERIALS are gratefully acknowledged.

In addition, the authors thank Jing Su who contributed to this study during her time in Regina.

This article is available online at AIST.org for 30 days following publication.

References

- 1. Gladman, T., The Physical Metallurgy of Microalloyed Steels, Maney Publishing, No. 615, 1997.
- 2. Baker, T.N., "Microalloyed Steels," Ironmaking & Steelmaking, Vol. 43, No. 4, 2016, pp. 264-307.
- 3. Gaudet, M.J.; Rashid, M.; van der Breggen, A.; Dunnett, K.; and Arafin, M., "X80 Heavy Gauge and Large Diameter Helical Line Pipe for Low Temperature Applications," *International Pipeline Conference*, American Society of Mechanical Engineers, Vol. 86588, 2022, p. V003T05A019.
- 4. Su, J.; Gaudet, M.; Konar, B.; Amirkhiz, B.S.; Fazeli, F.; Rashid, M.; and Arafin, M., "Effect of Through-Thickness Microstructure and Texture on Low-Temperature Toughness of Heavy-Gauge API X70 Linepipe Steels," *Metallurgical and Materials Transactions A*, Vol. 55, No. 8, 2024, pp. 2718–2735.
- 5. Gaudet, M.J., and Good, L., "A Study on Phase Transformation During Accelerated Cooling and Coiling of Line Pipe Steel," 3rd International Symposium on the Recent Developments in Plate Steels, Vail, Colo., USA, 2024.
- Sanz, L.; Pereda, B.; and López, B., "Effect of Thermomechanical Treatment and Coiling Temperature on the Strengthening Mechanisms of Low Carbon Steels Microalloyed With Nb," *Materials Science and Engineering: A*, Vol. 685, 2017, pp. 377–390.
- Wiskel, J.B.; Li, X.; Ivey, D.G.; and Henein, H., "Characterization of X80 and X100 Microalloyed Pipeline Steel Using Quantitative X-Ray Diffraction," Metallurgical and Materials Transactions B, Vol. 49, 2018, pp. 1597–1611.
- 8. Bakkaloğlu, A., "Effect of Processing Parameters on the Microstructure and Properties of an Nb Microalloyed Steel," *Materials Letters*, Vol. 56, No. 3, 2002, pp. 200–209.
- 9. Jia, T., and Militzer, M., "The Effect of Solute Nb on the Austenite-to-Ferrite Transformation," *Metallurgical and Materials Transactions A*, Vol. 46, 2015, pp. 614–621.
- 10. Bansal, G.; Srivastava, V.; and Chowdhury, S.G., "Role of Solute Nb in Altering Phase Transformations During Continuous Cooling of a Low-Carbon Steel," *Materials Science and Engineering: A, Vol. 767*, 2019, p. 138416.
- 11. Maetz, J.Y., et al., "Modeling of Precipitation Hardening During Coiling of Nb-Mo Steels," Metals, Vol. 8, No. 10, 2018, p. 758.
- 12. Raj, R.; Wiskel, J.B.; Gaudet, M.J.; Ivey, D.G.; and Henein, H., "The Effect of Non-Uniform Skelp Temperature on X70 Steel Coil Cooling," *Ironmaking & Steelmaking*, 2024.
- Andersson, J.O.; Helander, T.; Höglund, L.; Shi, P.; and Sundman, B., "Thermo-Calc & DICTRA, Computational Tools for Materials Science," Calphad, Vol. 26, No. 2, 2002, pp. 273–312.
- 14. Bai, D.; Bodnar, R.; Ward, J.; Dorricott, J.; and Sanders, S., "Development of Discrete X80 Line Pipe Plate at SSAB Americas," *International Symposium on the Recent Developments in Plate Steels*, 2011, pp. 13–22.
- Ouchi, C.; Sampei, T.; and Kozasu, I., "The Effect of Hot Rolling Condition and Chemical Composition on the Onset Temperature of γ-α Transformation After Hot Rolling," *Transactions of the Iron and Steel Institute of Japan*, pp. 22, No. 3, 1982, pp. 214–222.
- 16. American Petroleum Institute, API RP 5L3(R2020): Drop-Weight Tear Tests on Line Pipe, 4th Edition, 2020.
- 17. Schindelin, J.; Arganda-Carreras, I.; Frise, E.; Kaynig, V.; Longair, M.; Pietzsch, T.; Preibisch, S.; Rueden, C.; Saalfeld, S.; Schmid, B.; and Tinevez, J.Y., "Fiji: An Open-Source Platform for Biological-Image Analysis," *Nature Methods*, Vol. 9, No. 7, 2012, pp. 676–682.
- 18. Petrov, R.H.; Jonas, J.J.; Kestens, L.A.; and Gray, J.M., "Microstructure and Texture Development in Pipeline Steels," *Oil and Gas Pipelines*, 2015, pp. 157–186.
- 19. Jonas, J.J., "Transformation Textures Associated With Steel Processing," *Microstructure and Texture in Steels: And Other Materials*, Springer London, London, U.K., 2009, pp. 3–17.

